ELSEVIER

Journal of Power Sources 64 (1997) 181–187

JOURNAL OF POWER SOURCES

Modelling of local conditions in flooded lead/acid batteries in photovoltaic systems

Dirk Uwe Sauer

Fraunhofer Institute for Solar Energy Systems ISE, Oltmannsstrasse 5, 79100 Freiburg, Germany

Abstract

A model is set up for a time-dependent description of currents, polarizations, state-of-charge and acid concentration with high spatial resolution in a flooded lead/acid battery. The detailed description of all relevant parameters for a battery under real operating conditions allows the use of results obtained under well-characterized laboratory conditions for different ageing effects. Models of acid stratification, vertical current distribution in the electrode, and description of polarizations, concentrations and state-of-charge in the porous electrodes are necessary for any ageing model. First results show the very severe conditions for the lower part of the electrode under typical operating conditions in photovoltaic power supply systems. The work aims at a quantitative ageing model for batteries in such systems.

Keywords: Lead/acid batteries; Modelling; Stratification; Current distribution; Ageing; Photovoltaic systems

1. Introduction

Predicting the ageing of a battery under real and non regular operating conditions is still characterized more by expert experience than by quantitative models, even though many ageing processes in flooded lead/acid batteries are well understood.

Laboratory experiments under well-known conditions were performed and theoretical models were developed over the past hundred years. The goal of this work is to enable the use of these experiences for an ageing model for batteries under real operating conditions, especially in photovoltaic (PV) systems.

Accelerated ageing effects of lead/acid batteries are observed in almost all stand-alone PV systems around the world [1–3]. There are two ways to extend the battery lifetime. The first is to construct special batteries meeting the requirements of PV systems and the second is to improve the system design and control strategies to meet the requirement of existing batteries. To improve control strategies through computer simulation, a detailed ageing model is necessary. Even though it is clear that the ageing effects are correlated e.g. with the end-of-charge voltage and long periods in deep-discharged states, no quantitative descriptions of these correlations are available. This paper describes a combination of different models to allow simulation and calculation of ageing effects in flooded lead/acid batteries. Initially, this helps to optimize calculations of control strategies but it also provides information for appropriate battery construction.

The two main parts of the ageing model for flooded lead/acid batteries are:

1. Description of all relevant parameters, including polarization, current density, acid concentration and state-of-charge (SOC) at any time and position in flooded lead/acid batteries.
2. Using laboratory results of individual electrochemical effects obtained under well-known conditions and correlating them with knowledge of known conditions in the battery of a PV system.

For the first part, the following steps are necessary:

(i) modelling of acid stratification in the flooded cells;

(ii) macroscopic modelling of the current/voltage relation, taking the acid stratification into account, and

(iii) microscopic modelling of polarization, current and acid concentration of the porous electrodes.

Results from these parts of the model and the algorithms are given in this paper. The concepts are outlined for parts (i) and (iii) and part (ii) is discussed in more detail. A time-dependent description with high spatial resolution of all relevant parameters is available with this model. All models are developed such that a minimum number of experimental parameters are needed to calibrate the models. This allows easy application to a great number of batteries and operating conditions, without time-consuming and expensive laboratory experiments.

PII S0378-7753(96)02519-0

2. Acid stratification

Acid stratification occurs in flooded lead/acid batteries as well as in valve-regulated lead/acid (VRLA) batteries (especially absorbent glass mat AGM) under the typical conditions of a PV system [2] and is described by Apateanu et al. [4] and Armenta [5]. The acid concentration influences ageing effects, e.g. corrosion and sulfation, and the current distribution in the electrodes. Therefore, a model is developed to simulate acid stratification in flooded lead/acid batteries.

Input data for the model are geometric parameters of the cell and the electrodes, nominal acid volume and density and time series of battery current and temperature. The model takes temperature effects, the Ah efficiency as a function of battery voltage and temperature [7] and the loss of water through gassing into consideration.

The model consists of three main parts: (i) diffusion due to concentration gradients; (ii) buoyancy due to differences in specific gravity, and (iii) acid circulation due to gassing effects.

The ideas of the different parts are shown in the following sections.

2.1. Simulation grid

The effects are calculated on a discrete simulation grid. Fig. 1 shows an example of the grid used for all calculations of the stratification model. In the example, a battery with two electrodes (one positive, one negative) is shown, but any battery geometry and number of electrodes can be modelled. The size of a volume element depends on the location in the battery. Each volume element (VE) is characterized by its volume V, the length l, the height h, the width b, the number M of moles H_2SO_4 contained in the volume element, the temperature and the position in the grid.

Diffusion, buoyancy and circulation due to gassing is calculated on this grid. All volume elements have the length l, which is the depth of the battery. Therefore, a two dimensional density distribution is calculated. The electrodes are assumed compact and the pore volume is taken as a part of the free electrolyte volume between the electrodes. The acid distribution in the porous electrodes is modelled in more detail by the electrode model described in Section 5. The volume of all volume elements remains constant within the complete simulation, except the volume elements above the electrodes. Due to gassing, the electrolyte level decreases or increases after topping-up of the battery. Therefore the height h of the volume elements above the electrodes is adjusted continuously to the electrolyte level. Another reason for changes of the electrolyte level are temperature effects. The volume elements next to the electrodes serve as a source or sink of H_2SO_4 molecules during charging respectively discharging of the battery.

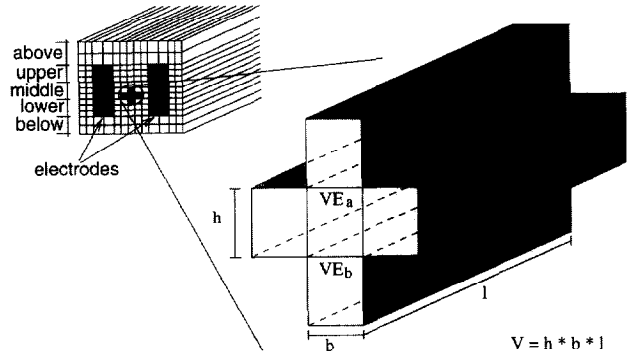

Fig. 1. Example of a simulation grid used for a battery with one positive and one negative electrode. Each volume element (VE) is characterized by its volume V, the length l (l is also the depth of the battery), the height h, the width b and the number M of moles H_2SO_4 contained in the VE.

2.2. Diffusion

Diffusion between two volume elements is given by Fick's first law

$$j = -D\frac{dc}{dx} \tag{1}$$

where j is the flow rate, D the diffusion coefficient of H_2SO_4, x the distance and c the concentration of H_2SO_4. The number of moles H_2SO_4 exchanged by diffusion between two volume elements VE_a and VE_b during the time Δt is given by

$$M_b = \frac{\left(\frac{M_a}{V_a} - \frac{M_b}{V_b}\right)(V_a V_b)}{V_a + V_b} \times \left[1 - \exp\left(-D\frac{A}{\Delta x}\frac{V_a + V_b}{V_a V_b}\Delta t\right)\right] \quad \Delta M_a = -\Delta M_b \tag{2}$$

where $\Delta x = h$ is the distance between the centres of the volume elements and $A = bl$ is the area of the common surface between the two volume elements. The diffusion is calculated between all neighbouring volume elements.

2.3. Buoyancy

Density gradients are caused by the release of highly concentrated acid from the electrodes during charging and depletion of the acid close to the electrodes during discharging, according to the electrode reactions. For modelling the buoyancy due to density differences, it is assumed that a certain volume element (VE) with density ρ_a is surrounded by a liquid with density ρ_b. Density ρ_b is taken from VE_b located below VE_a, if $\rho_a > \rho_b$. The liquid from VE_a moves the distance Δx during the time interval Δt into VE_b, and vice versa

$$\Delta x = \frac{8gb^2}{\eta}\Delta t(\rho_a - \rho_b) \tag{3}$$

where η is the viscosity, g the standard acceleration due to gravity and b a geometric parameter. In the zone Δx, the liquids of VE_a and VE_b are intermixed. This results in a change in the moles H_2SO_4 in VE_a and VE_b after the time interval Δt given by Eq. (4)

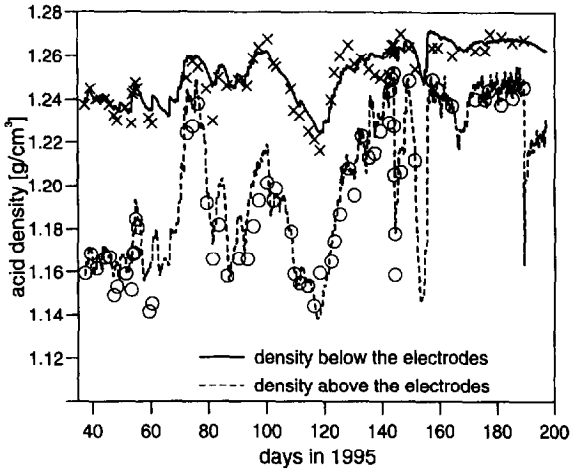

Fig. 2. Acid density above the electrodes and below the electrodes over a period of 160 days in a battery cell (2 V, 200 Ah, 4 positive tubular electrodes and 5 negative flat plate electrodes) under typical operating conditions in a stand-alone PV system. The lines are calculated from the presented model with time series of current and battery temperature as input data. The points are results from manual measurements in the battery. At the 190th day topping-up of the battery occurred.

$$\Delta M_a = \frac{M_b V_a \Delta x}{2 h_a V_b} - \frac{M_a \Delta x}{2 h_a} \quad \Delta M_b = -\Delta M_a \tag{4}$$

2.4. Gassing

The electrolyte in the battery is mixed by gassing. The gas flow is calculated with Tafel's temperature and voltage dependent Eq. (6). Stoichiometric gassing is assumed, which originates uniformly over the electrodes geometric surfaces. The gas flow of O_2 and H_2 through each volume element is calculated. The gas volume flow depends on the produced gas molecules in the time interval Δt, the local pressure and the temperature. It is assumed, that the gas displaces the electrolyte resulting in an exchange of liquid between vertically adjacent volume elements. The exchange rate depends only on the gas volume, not on the number nor on the size of the gas bubbles. The strength of the mixing effect is described by a linear coefficient f_{gas}, which was found to be 0.2 by comparing experimental and simulation data.

The exchange of moles H_2SO_4 in VE_a and VE_b is given by Eq. (5)

$$\Delta M_a = V_{gas} f_{gas} \left(\frac{M_b}{V_b} - \frac{M_a}{V_b} \right) \quad \Delta M_b = -\Delta M_a \tag{5}$$

where V_{gas} is the gas volume flowing through the volume elements during the time interval Δt.

2.5. Results

A time-step simulation is performed for the modelling of the acid stratification. During each time step the exchange of moles H_2SO_4 between adjacent volume elements through the three described effects is calculated and this gives the new number of moles in each volume element. The electrolyte density is related to the number of moles in and the volume of the volume element.

The complete model predicts the strength and influence of acid stratification as a function of the geometric parameters of the cell and as a function of operating conditions and control strategies.

Fig. 2 shows the result of a comparison between the model's results with data from the battery of the Self Sufficient Solar House, Freiburg, Germany [7,8] (48 V/400 Ah, 2.5 years in operation in a PV system, 200 Ah cells, electrode height 28 cm) and manual measurements of the acid density over a period of 160 days. Only densities above and below the electrodes are shown. The densities between the electrodes at different heights are measured and simulated as well. Table 1 presents statistics of the comparison between the measured and the simulated data in the regions above and below the electrodes, and in the upper, middle and lower section of the electrodes. The simulation was carried out with the measured time series of battery current, temperature and voltage. The first measured densities were taken as starting points for the simulation.

It is obvious from Table 1 that the simulated data are in good agreement with the measured data except at the lower section of the electrodes. Visual inspection and analysis of the measured electrical and density data show that accelerated ageing of the lower part of the electrodes is highly significant.

Table 1
Statistics on the comparison of 65 density measurements $\rho^{i,j}_{measure}$ at 5 positions with respect to the electrodes (Fig. 1) with simulated data $\rho^{i,j}_{sim}$ from time series of current and temperature over a period of 160 days (compare with Fig. 2, all values in g/cm³). Different statistical measures are calculated, to show systematic and statistical deviations between simulated and measured data. The resolution of the used manual density meter is about 0.0025 g/cm³

j	Position	$\frac{1}{65}\sum_{i=1}^{65} \lvert \rho^{i,j}_{sim} - \rho^{i,j}_{measured} \rvert$	$\frac{1}{65}\sum_{i=1}^{65} \lvert \rho^{i,j}_{measured} - \rho^{i,j}_{sim} \rvert$	$\sqrt{\frac{\sum_{i=1}^{65} (\rho^{i,j}_{sim} - \rho^{i,j}_{measured})^2}{64}}$
1	Below	0.0043	0.0017	0.0056
2	Lower	0.0163	−0.0154	0.0224
3	Middle	0.0065	−0.0015	0.0084
4	Upper	0.0051	−0.0004	0.0063
5	Above	0.0079	0.0066	0.0107

This results in a growth of the negative electrode, probably caused by irreversible sulfation, and therefore a decrease of the local capacity. This changes the geometric and electrical properties in the lower part of the electrode. Therefore, the assumption of a homogeneous electrode is no longer valid.

The model is stable for different starting conditions. After a few days, the simulated stratification is similar to the results obtained with the measured starting conditions, even though arbitrary starting conditions were chosen, as long as the mean concentration of the electrolyte is represented exactly. Also, the results are almost independent of the number of volume elements chosen. A minimum number of volume elements between the electrodes of six in the horizontal and nine in the vertical direction is necessary.

3. Electric circuit model

As a result of acid stratification, different electrochemical potentials appear at different heights of the electrode. The electrochemical potential of the $Pb/H_2SO_4/PbO_2$ system is given by [9]

$$V_0(V) = 2.048[V] + \frac{RT}{2F}\log\left(\frac{4f_{\pm}^3 c_{H_2SO_4}^3}{a_{H_2O}}\right) \quad (6)$$

where R is the universal gas constant, T the absolute temperature, F the Faraday constant, $f_{\pm}$ the mean activity coefficient of sulfuric acid, $c_{H_2SO_4}$ the acid concentration and $a_{H_2SO_4}$ the activity of H_2O. A well-known linaer approximation of Eq. (6) is the rule of thumb for the electrochemical potential

$$V_0(V) = 0.84[V] + \rho \quad (7)$$

where ρ is the density of the electrolyte in g/cm^3. Eq. (7) shows that differences in density of 0.01 g/cm^3 result in differences in the electrochemical potential of 10 mV.

Electric circuit models are often used for the calculation of the current–voltage relation of lead/acid batteries. To take effects of acid stratification into account, an extension of an electric circuit for a high spatial resolution is necessary. Therefore, the electrodes are divided into three parallel circuits (upper, middle and lower part of the electrode), each with its own electrochemical voltage source. The local electrochemical potential depends on the acid density (or concentration) and results in inhomogeneous currents at different heights of the battery and thus in different local SOCs (Fig. 3). Three parallel circuits were chosen, because the resulting equations of this model can be solved in an explicit formulation and the realistic spatial resolution of the stratification model is in the same range.

R_a, R_b and R_c represent the grid and the connector resistances of the electrodes. R_1, R_2 and R_3 depend on the local electrolyte resistance and therefore on the acid concentration and temperature plus a constant resistance value (different values during charging and discharging). $U_{SP,1}$, $U_{SP,2}$ and $U_{SP,3}$ are the electrochemical potentials according to Eq. (6).

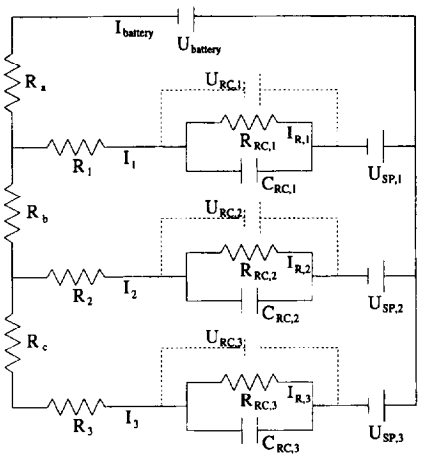

Fig. 3. Electric circuit for simulation of current–voltage relation considering the influence of acid stratification. R_1, R_2, R_3 depend on the local acid concentration and, therefore, the electrolyte resistance. R_a, R_b, R_c represent resistance of the grid (positive and negative electrode together). $C_{RC,1}$, $C_{RC,2}$, $C_{RC,3}$ are capacitors with constant values. $R_{RC,1}$, $R_{RC,2}$, $R_{RC,2}$ depend on the local SOC in the way described by Shepherd [10]. $U_{SP,1}$, $U_{SP,2}$, $U_{SP,3}$ are voltage sources representing the electrochemical voltage depending on the local H_2SO_4 concentration. $I_{battery}$ and $U_{battery}$ are the terminal current and voltage of the battery.

$C_{RC,1}$, $C_{RC,2}$ and $C_{RC,3}$ are constant capacitors and $R_{RC,1}$, $R_{RC,2}$ and $R_{RC,3}$ are SOC dependent resistors. The SOC dependence is formulated following Shepherd [10]

$$R_{RC,i} = \frac{R_{RCE,i}(K_{RCQL,i} - Q_i)}{K_{RCQE,i} - (1 - Q_i)} \text{ during discharging} \quad (8)$$

$$R_{RC,i} = \frac{R_{RCL,i} Q_i}{K_{RCQL,i} - Q_i} \text{ during charging} \quad (9)$$

$$Q_i = Q_i^0 + \frac{1}{C_{10}^{local}} \int_{t=0}^{t} (I_i - I_{gas})\,dt' \quad (10)$$

where $R_{RCE,i}$, $K_{RCQL,i}$, $K_{RCQE,i}$ and $R_{RCL,i}$ are parameters according to Shepherd's formulation and Q_i is the local SOC calculated with a temperature and voltage dependend gassing current I_{gas} [6] and the local capacity $C_{10}^{local} = 1/3C_{10}$.

For a new and fully charged battery with a homogeneous electrolyte, the following relations are valid: $R_b = R_c$, R_a includes additional to R_b and R_c the resistance of the poles, $C_{RC,1} = C_{RC,2} = C_{RC,3}$, $R_1 = R_2 = R_3$, $R_{RC,1} = R_{RC,2} = R_{RC,3}$.

The values can be calculated by fitting the model to measured data (SOC, electrolyte density, terminal voltage and current, and battery temperature). We use a genetic algorithm to fit the parameters [11].

$I_{battery}$ and $U_{battery}$ are the terminal current and voltage, with one value being determined by the operating conditions (constant voltage or constant current mode).

The electric circuit is solved explicitly with Kirchhoff's laws. The RC terms are solved in a first step separately. $U_{RC,1}$, $U_{RC,2}$ and $U_{RC,3}$ are taken as separate circuits with currents I_1, I_2 and I_3. This results in the following equations

$$U_{RC,i}(t) = -\frac{-Q^0_{RC,i} + C_{RC,i}R_{RC,i}I_i - C_{RC,i}R_{RC,i}I_i \exp(t/C_{RC,i}R_{RC,i})}{C_{RC,i}\exp(t/C_{RC,i}R_{RC,i})} \quad (11)$$

$$I_{R,i}(t) = -\frac{-Q^0_{RC,i} + C_{RC,i}R_{RC,i}I_i - C_{RC,i}R_{RC,i}I_i \exp(t/C_{RC,i}R_{RC,i})}{C_{RC,i}\exp(t/C_{RC,i}R_{RC,i})} \quad (12)$$

$$Q_{RC,i}(t) = C_{RC,i}R_{RC,i}I_i + \frac{Q^0_{RC,i} - C_{RC,i}R_{RC,i}I_i}{\exp(t/C_{RC,i}R_{RC,i})} \quad (13)$$

With these results the complete circuit can be described by four independent equations given again by Kirchhoff's laws, where $U_{RC,1}$, $U_{RC,2}$ and $U_{RC,3}$ are taken from Eq. (11)

$$0 = -U_{battery} + U_{RC,1} + U_{SP,1} + R_1 I_1 + R_a I_{battery} \quad (14)$$

$$0 = -R_1 I_1 - U_{RC,1} - U_{SP,1} + U_{SP,2} + U_{RC,2} + R_2 I_2 + R_b(I_2 + I_g) \quad (15)$$

$$0 = -R_2 I_2 - U_{RC,2} - U_{SP,3} + U_{SP,3} + U_{RC,3} + R_3 I_3 + R_c I_3 \quad (16)$$

$$0 = I_{battery} - I_1 - I_2 - I_3 \quad (17)$$

Eqs. (14)–(17) are solved for I_1, I_2, I_3 and $I_{battery}$ respectively $U_{battery}$ (Eqs. (18)–(21),) explicitly. Because of extensive calculations the software package Mathematica [12] was used

$$I_i = f(U_{battery}, t, \{\text{set of parameters}\}, \{U_{SP,1}, U_{SP,2}\ U_{SP,3}\}) \quad (18)$$

$$I_{battery} = f(U_{battery}, t, \{\text{set of parameters}\}, \{U_{SP,1}, U_{SP,2}\ U_{SP,3}\}) \quad (19)$$

or

$$I_i = f(I_{battery}, t, \{\text{set of parameters}\}, \{U_{SP,1}, U_{SP,2}\ U_{SP,3}\}) \quad (20)$$

$$U_{battery} = f(I_{battery}, t, \{\text{set of parameters}\}, \{U_{SP,1}, U_{SP,2}\ U_{SP,3}\}) \quad (21)$$

Eqs. (18) and (19) are used in the constant voltage mode, Eqs. (20) and (21) in the constant current mode.

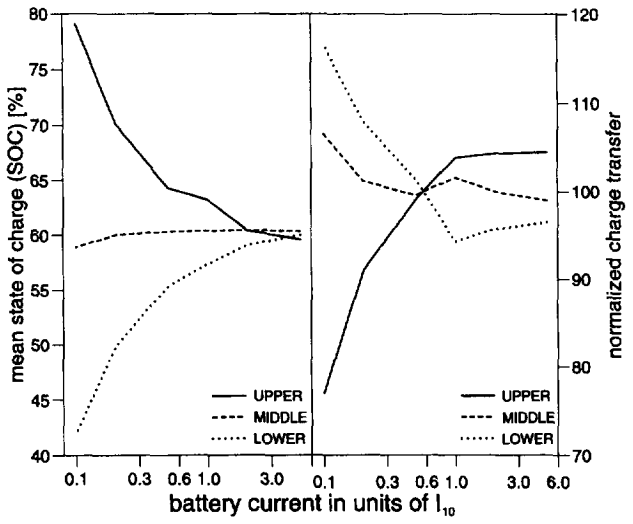

Fig. 4. Mean SOC and normalized charge transfer over 20 consecutive constant-current charge and discharge cycles between 90% and 30% SOC as a function of the battery current for the upper, middle and lower parts of the electrode. The acid density was taken in the upper part 0.01 g/cm^3 below and in the lower part 0.01 g/cm^3 above the SOC-dependent mean density, to simulate a moderate acid stratification.

Parameters of the model were fitted to measured data from a 2.5-year old battery [7,8] (200 Ah cells, tubular plate positive electrodes). Fig. 4 shows the influence of inhomogeneous electrolyte densities in the battery. The density at the upper part of the electrode was set 0.01 g/cm^3 lower then the SOC-dependent mean density. For the lower part, it was set to 0.01 g/cm^3 above the mean density, while the middle part had the mean density all the time. Twenty consecutive partial charging and discharging cycles (between SOC = 90% and SOC = 30%) at constant currents (constant voltage mode at voltages above 2.5 V) were performed in the simulation. Charge transfer and mean SOC were calculated for different applied battery currents. The results are plotted in Fig. 4. The left-hand figure shows the mean SOC as a function of the current and the right-hand figure the normalized charge transfer. For currents greater than I_{10}, the mean SOC is almost equal at all parts of the electrodes and charge transfer is a little bit higher in the upper part of the electrode. This is a result of the grid resistance, as already predicted in 1965 by Euler and Horn [13]. However, for currents less than I_{10}, the mean SOC starts to differ more and more. The lower part of the electrode shows a steadily decreasing mean SOC with decreasing currents. At the same time, the charge transfer in this region increases.

The explanation for this behaviour lies in the small polarizations at low currents. The voltage difference caused by the inhomogeneous electrolyte concentration becomes more important in relation to the polarization caused by the currents. During discharge cycles, the lower part of the electrode is discharged with higher currents than the upper part because of the higher electrochemical potential. During charging, the upper part is charged first, because of the lower electrochemical potential. The effect increases for higher stratification and smaller currents and vanishes for a battery with a homogeneous electrolyte or at high currents.

The chosen cycling regime may appear to be atypical, but in fact cycles like these happen in PV systems very often at currents in the range from I_{10} to I_{100}. (see Ref. [8] for typical operating conditions of batteries in PV systems). This cycling regime was used to demonstrate the predictions of the electrical model. It shows the very severe conditions for the lower parts of the electrodes in batteries with acid stratification and low currents as they occur very often in PV systems.

For future investigations the stratification model and the electric model will be combined. Local acid densities are given by the stratification model and the vertical current distribution within the electrode is given by the electric circuit model. Experiments have now been started to verify the predictions of the model.

4. Electrode model

The coupled stratification and electric circuit model gives the current and acid concentration distribution in the vertical direction. However, there are also inhomogeneities in the horizontal direction of the electrodes. Due to acid transportation through the porous electrodes, local acid concentrations, polarizations and SOCs are functions of the distance to the grid. The effects depend on the currents and the geometry of the electrode.

A formulation presented in 1973 by Simonsson [14] is used for simulating distributions of polarization η, current i and concentration c in the electrode. A system of coupled partial differential equations describing diffusion, migration and convection for the discharge process is solved with numerical methods

$$\frac{\partial\eta(z,t)}{\partial z}=f\left(\frac{\partial E}{\partial c},\frac{\partial c(z,t)}{\partial z},\, i,\, \{\text{set of parameters}\}\right) \tag{22}$$

$$\frac{\partial c(z,t)}{\partial t}=f\left(\frac{\partial i(z,t)}{\partial z},\frac{\partial^2 c(z,t)}{\partial z^2},\frac{\partial c(z,t)}{\partial z},\, i,\, \{\text{set of parameters}\}\right) \tag{23}$$

$$\frac{\partial i(z,t)}{\partial z}=f(X(z,t),\exp(\eta(z,t))) \tag{24}$$

$$X(z,t)=f\left(\int_{t_0}^{t}\frac{\partial i(z,t)}{\partial z}\mathrm{d}t'\right) \tag{25}$$

where the parameters include dependencies on the geometry of the electrode, diffusion coefficients of different species, porosities and specific volumes. $\partial E/\partial c$ is the gradient of the electrochemical potential with respect to concentration, z the distance from the grid, i the current, t the discharge time and X the local SOC. With slight modifications of the equations and the parameters, the model can be used for charging and discharging in a dynamic approach. This allows the dynamic simulation of real operating conditions of batteries in PV systems.

As an example, Fig. 5 shows local SOCs within a charge and discharge cycle with $2I_{10}$ (Fig. 5(a)) and $0.5I_{10}$ (Fig. 5(b)). The local SOC is expressed in local PbO_2 content in relation to the PbO_2 content in a fully charged battery, where a 100% content of PbO_2 in the fully charged battery is assumed.

Detailed information about local SOCs, acid concentrations, polarizations and currents within the active mass are obtained from this part of the model as a function of the horizontal distance from the grid.

5. Outlook

The final goal of the modelling is the formulation of a quantitative ageing model for lead/acid batteries with special

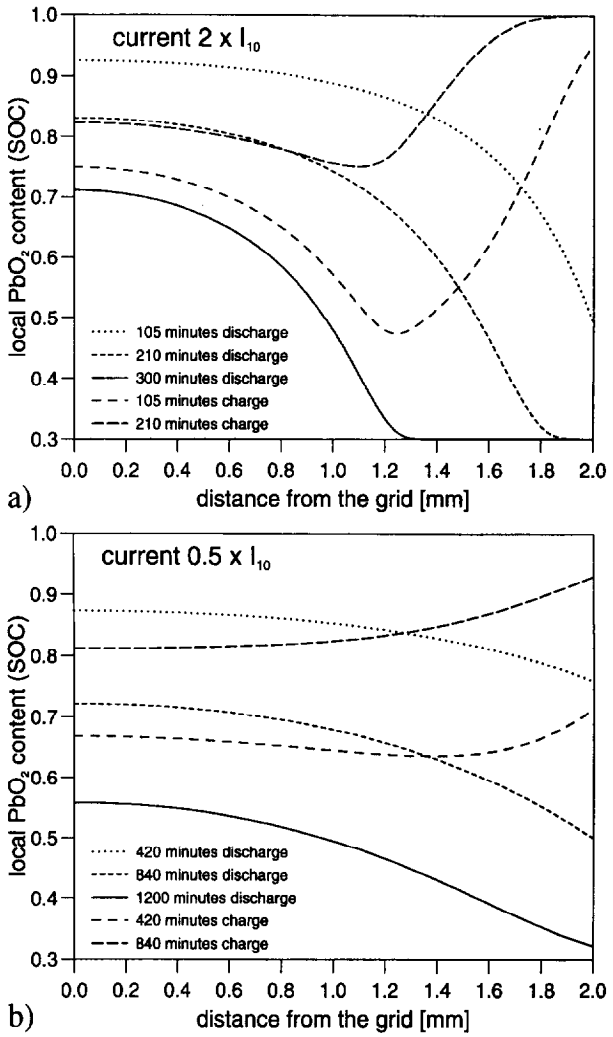

Fig. 5. Local SOC between the grid and the free electrolyte of an electrode while discharging and charging with constant-current (current in (a) is $2I_{10}$, in (b) $0.5I_{10}$). From the fully charged electrode, 50 Ah were discharged and then 50 Ah recharged (nominal capacity approximately 50 Ah) within 5 or 20 h, respectively.

respect to typical operating conditions in PV systems [8]. The detailed description of the parameters polarization, current, acid density and SOC allows the use of results obtained under well-known laboratory conditions for different ageing effects.

In the past decades, several investigations on ageing effects such as corrosion and sulfation were performed, e.g. corrosion of lead as a function of the voltage and acid concentration [15], corrosion of lead with and without active material around it [16], crystallization processes of $PbSO_4$ [17,18], premature capacity loss (PCL) [19] or the development of structures in the active mass during cycling [18].

The corrosion rate given by Lander [15] was the starting point for a simple ageing model developed by Degner et al. [20], which serves as a model for our future work.

6. Conclusions

By combining the stratification and electric circuit models with extra information from the electrode model, the condi-

tions in the battery and the electrodes at every place and time are predictable. A minimum number of experimental data are necessary to calibrate the models. As far as possible, all effects are described by physical contexts. This allows an easy use for various types of batteries.

Calculations have shown, that the typical operating conditions of PV systems lead to very severe conditions for the lower part of the electrodes. This is caused mainly by the irregular vertical current distribution due to acid stratification.

This model gives the oppurtunity to use results from various laboratory experiments under well-known conditions for ageing simulations of real operating conditions. This also facilitates the calculation of an optimum control strategy and system layout for any special purpose, e.g. battery size, end-of-charge voltage and end-of-discharge thresholds for batteries in PV systems. Further use can be made by battery manufacturers of the model's predictions to develop a more sophisticated battery design.

Acknowledgements

This project is supported by the German Ministry of Education and Research (BMBF).

References

[1] S. McCarthy, A. Kovach and G.T. Wrixon, *9th European Photovoltaic Solar Energy Conf., Freiburg, Germany, 1989*, pp. 1142–1145.

[2] H. Döring, A. Jossen, D. Köstner and J. Garche, *10th Symp. Photovoltaische Solarenergie, Staffelstein, Germany, 1995*, pp. 549–553.

[3] A.F. Hollenkamp, W.G.A. Baldsing, J.A. Hamilton and D.A.J. Rand, *J. Power Sources, 31* (1990) 329–336.

[4] L. Apateanu, A.F. Hollenkamp and M.J. Koop, *J. Power Sources, 46* (1993) 49–60.

[5] C. Armenta, *Solar Wind Technol., 6* (5) (1989) 541–549.

[6] G. Bopp, H. Gabler, D.U. Sauer, A. Jossen, W. Höhe, J. Mittermeier, M. Bächler, P. Sprau, B. Willer and M. Wollny, *13th European Photovoltaic Solar Energy Conf., Nice, France, 1995*, Vol. 2, pp. 1763–1769.

[7] A. Armbruster, G. Bopp, A. Goetzberger, H. Lehmberg, J. Luther and K. Voss, *13th European Photovoltaic Solar Energy Conf., Nice, France, 1995*, Vol. 1, pp. 360–363.

[8] D.U. Sauer, M. Bächler, G. Bopp, W. Höhe, J. Mitermeier, P. Sprau, B. Willer and M. Wollny, *J. Power Sources, 64* (1997) 197–201.

[9] D. Berndt, *Blei-Akkumulatoren*, VDI Verlag, Düsseldorf, 11th edn., 1986

[10] C.M. Shepherd, *J. Electrochem. Soc., 112* (1965) 657–664.

[11] L. Davis, *Handbook of Genetic Algorithms*, Van Nostrand Reinhold, New York, 1991.

[12] *Mathematica 2.2 for HP9000 Series 700*, Copyright 1988–93 Wolfram Research.

[13] J. Euler and L. Horn, *Arch. Elektrotech. (Berlin), 50* (1965) 85–90.

[14] D. Simonsson, *J. Appl. Electrochem., 3* (1973) 261–270.

[15] J.J. Lander, *J. Electrochem. Soc., 103* (1956) 1–8.

[16] J. Garche, J. Power Sources, 53 (1995) 85–92.

[17] J. Burbank, A.C. Simon and E. Willihnganz, *Adv. Electrochem. Electrochem. Eng., 8* (4) (1971) 157–251.

[18] D. Pavlow and E. Bashtavelova, *J. Electrochem. Soc., 133* (1986) 241–248.

[19] A.F. Hollenkamp, K.K. Constanti, A.M. Huey, M.J. Koop and L. Apateanu, *J. Power Sources, 40* (1992) 125–136.

[20] T. Degner, H. Gabler and A. Stöcklein, *12th European Photovoltaic Solar Energy Conf., Amsterdam, The Netherlands, 1994*, Vol. 1, pp. 422–426.